Supporting information for

A nickel/cobalt-free Mn-based layered oxide cathode based on orbital hybridization modulation strategy for high energy density sodium-ion batteries

Zhuozheng Hong,[a,b,†] Xin-Yu Zhang,[b,†] Minwen Yang,[c,†] Yan-Fang Zhu,[b] Diancheng Chen,[c] Yan-Jiang Li,[d] Haojie Dong,[e] Yaping Yan,[h,*] Yubin Niu,[f] Peng-Fei Wang,[e] Yang Sun,[c,*] Chao Wu,[a,*] and Yao Xiao[b,g,*],

a. Institute of Energy Materials Science (IEMS), University of Shanghai for Science and Technology, Shanghai, 200093, P. R. China. E-mail: chaowu@usst.edu.cn

b. College of Chemistry and Materials Engineering, Wenzhou University, Wenzhou, 325035 P. R. China. E-mail: xiaoyao@wzu.edu.cn.

c. School of Materials, Sun Yat-sen University, Shenzhen 518107, China. E-mail: sunyang5@mail.sysu.edu.cn.

d. Key Laboratory of Spin Electron and Nanomaterials of Anhui Higher Education Institutes, Suzhou University, Suzhou 234000, China.

e. Center of Nanomaterials for Renewable Energy, State Key Laboratory of Electrical Insulation and Power Equipment, School of Electrical Engineering, Xi'an Jiaotong University, Xi'an, Shaanxi 710049, P.R. China.

f. School of Materials and Energy, Southwest University, Chongqing, 400715 P. R. China.

g. State Key Laboratory of Critical Metals Beneficiation, Metallurgy and Purification, Zhengzhou University, Zhengzhou, Henan, 450002, P. R. China.

h. Henan Engineering Technology Research Center for Fiber Preparation and Modification, Henan International Joint Laboratory of Rare Earth Composite Materials, Henan University of Engineering, Zhengzhou, Henan, 451191 P. R. China. E-mail: yyp1990@haue.edu.cn.

AUTHOR INFORMATION

***Corresponding Author**

yyp1990@haue.edu.cn; sunyang5@mail.sysu.edu.cn; chaowu@usst.edu.cn; xiaoyao@wzu.edu.cn;

Experimental section

1. Chemical and materials

Sodium carbonate (Na_2CO_3, AR), Nickel oxide (NiO, AR), Magnesium oxide (MgO, AR), Iron oxide (Fe_2O_3, AR), Manganese oxide (MnO_2, AR), citric acid ($C_6H_8O_7$, ≥99.5%) were purchased from Aladdin Biochemical Technology Corp. All chemicals were used directly without further purification.

2. Material Synthesis

$Na_{0.55}Ni_{0.1}Fe_{0.1}Mn_{0.8}O_2$ and $Na_{0.55}Mg_{0.1}Fe_{0.1}Mn_{0.8}O_2$ powders were synthesized using a solid-state method. Initially, Na_2CO_3, NiO, MgO, Fe_2O_3, MnO_2 were ground together in stoichiometric ratios, with 10% excess Na_2CO_3 to compensate for volatilization at high temperatures. The powder was then pressed into 12 mm diameter discs at 20 MPa for 2 minutes and sintered at 1000°C for 15 hours in air. The discs were then cooled to room temperature to obtain the final product.

3. Materials Characterization

The samples were analyzed by x-ray diffraction (XRD) using a Bruker D8 Advance diffractometer (Rigaku D/max-2500) with a Cu Kα radiation source (λ = 1.5418 Å) in the range of 2θ = 10°~80°. The crystal structure was analyzed by Rietveld method using Fullprof software. The morphological and structural features were characterized by scanning electron microscopy (SEM, JEOL SU-8020, 10 kV). A special Swagelok cell with an ultra-thin aluminum window as an x-ray penetration window was used to collect in-situ charge-discharge XRDs in the range of 2θ = 10°~ 80° at a temperature of 0.1C. Synchrotron radiation X-ray absorption spectroscopy (XAS) measurements were conducted at the wiggler XAS Beamline (12ID) at the Australian Synchrotron in Melbourne, by using a set of liquid N_2 cooled Si (311) monochromator crystals. The morphological and structural peculiarities were characterized by transmission electron microscopy (TEM, JEOL JEM-2011, 200KV). Spherical aberration-corrected scanning transmission electron microscopy (STEM) (JEM-ARM200CF, JEOL, Tokyo, Japan). Electron paramagnetic resonance (EPR) experiments were performed using Bruker spectrometers (EMXplus-9.5/12).

Time-of-flight secondary ion mass spectroscopy (TOF-SIMS) was conducted on IONTOF M6 hybrid SIMS and the data were analyzed on Surface lab software. The TOF-SIMS tests were performed in negative-ion mode using a thermally ionized Cs ion source. The test area was a square with a side length of 100 um and the etching duration was 500 s. The etching rate was approximately 0.5 nm s^{-1}. Preparation of all samples for all ex-situ tests and cycled tests: the cells were disassembled to get the electrodes within 1 h after charging

and discharging. Immerse the electrodes in dimethylformamide (DMC) for 5 minutes, clean the residual glass fibers and electrolyte on the electrode sheet, and then store it in a glove box filled with argon gas.

4. Electrochemical tests

The electrochemical performance of half cells with NFM118 and MFM118 positive cathode materials was evaluated using coin cells (CR2032). The cells were fabricated in an argon-filled glove box. (1) Electrode preparation: the positive material, Super P carbon and polyvinylidene fluoride (PVDF) binder were dispersed in N-methyl pyrrolidone (NMP) in a ratio of 7:2:1 by mass and shaken well in an oscillating tube. The resulting slurry is uniformly coated onto the aluminum foil and transferred to a vacuum oven at 80 °C overnight. The mass loading of the cathode material in the resulting cathode pellet (10 mm diameter) was 2-3 mg/cm^2. (2) Battery assembly: sodium metal as a counter electrode, porous glass fibers as a diaphragm, and 1.0 M $NaClO_4$ (ethylene carbonate [EC]/diethyl carbonate [DEC] = 1:1 + 5 vol% fluorinated ethylene carbonate [FEC]) as electrolyte. (3) Battery testing: the coin cells were galvanostatic ally charge/discharge on a NEWARE Battery Test System (MIHW-200-160CH, Shenzhen, China) in the range of 1.5-4.3 V (1 C=160 mAh g^{-1}). CV was carried out on a Princeton instruments testing system and a GITT measurement was performed on the Neware test system[1].

The Na^+ diffusion coefficient (D_{Na^+}) calculation by CV results at different scan rates is according to the Randles-Sevcik equation:

$$I_P = 2.69 \times 10^5 n^{3/2} A C D_{Na^+}^{1/2} v^{1/2} \quad \text{(S1)}$$

where I_P represents the peak current (A), n represents the number of moles of electrons transferred in the reaction, C represents the Na^+ concentration in the lattice (mol cm^{-3}), A represents the area of electrode (cm^2), v represents the scan rate (V s^{-1})[2].

GITT was conducted by a galvanostatic current pulse of 0.2 C for 15 min, followed by an open circuit voltage relaxation time of 1 h. The Na^+ diffusion coefficient (D) calculation formula is[3]:

$$D = \frac{4}{\pi\tau}\left(\frac{m_B V_m}{M_B S}\right)^2\left(\frac{dE_s}{dE_\tau}\right)^2 \quad \text{(S2)}$$

5. DFT Calculation

All density functional theory (DFT) calculations were performed using the Vienna Ab initio Simulation Package (VASP). The interactions between ions and valence electrons were described using the Projector Augmented Wave (PAW) method. The exchange-correlation potential was treated within the generalized

gradient approximation (GGA) parameterized by Perdew-Burke-Ernzerhof (PBE)[4]. A plane-wave basis set with a cutoff energy of 480 eV was employed. The DFT+U method within the Dudarev formalism was adopted. The effective Hubbard parameters U_{eff} were set to 5.0 eV and 4.0 eV for the transition metal atoms, respectively. Spin-polarized calculations were performed, and the van der Waals (vdW) interactions were corrected using Grimme's DFT-D3 method. During the geometry optimization, both atomic positions and lattice constants were fully relaxed using the conjugate gradient algorithm until the Hellmann-Feynman forces on each atom were less than 0.02 eV/Å[5]. The convergence criterion for the total energy was set to $1◊10^5$ eV.

Results and Discussion

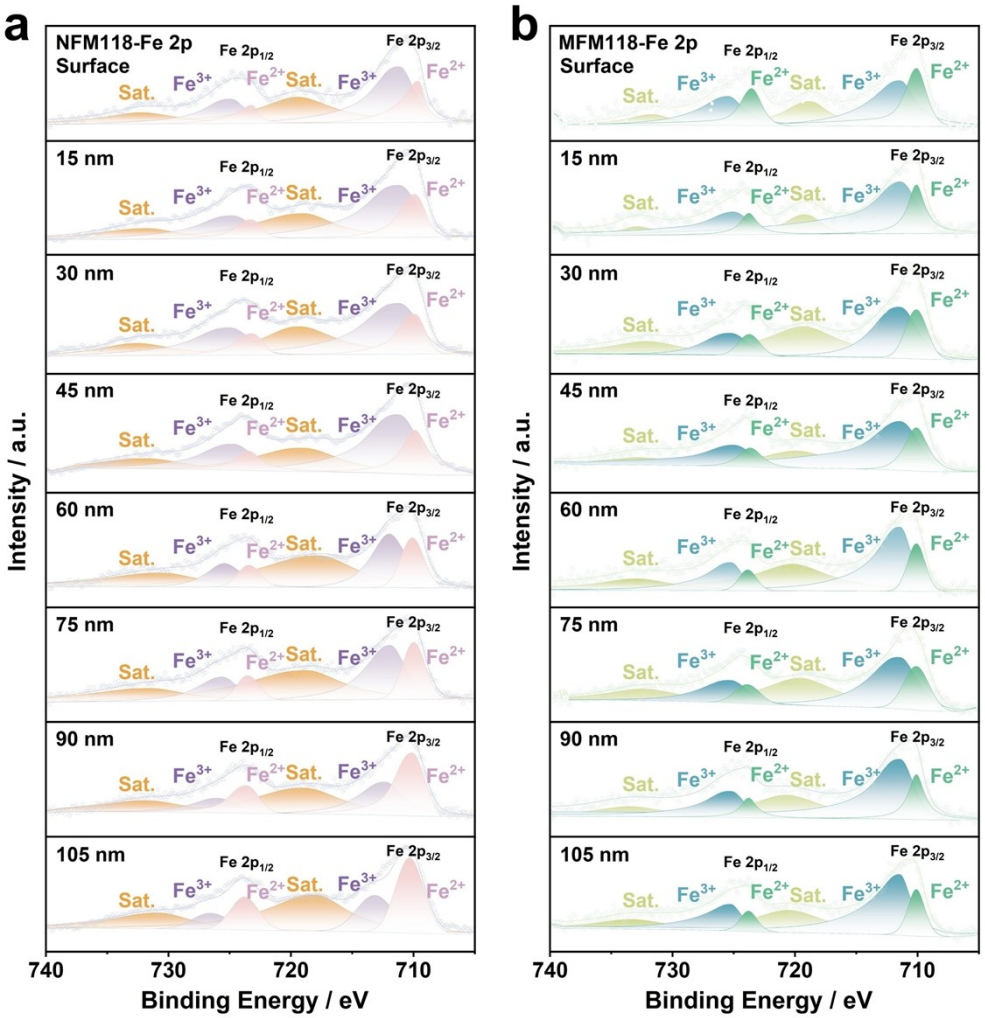

Figure S1. High resolution XPS spectra of (a) Fe 2p at surface of NFM118 pellets and (b) surface of MFM118.

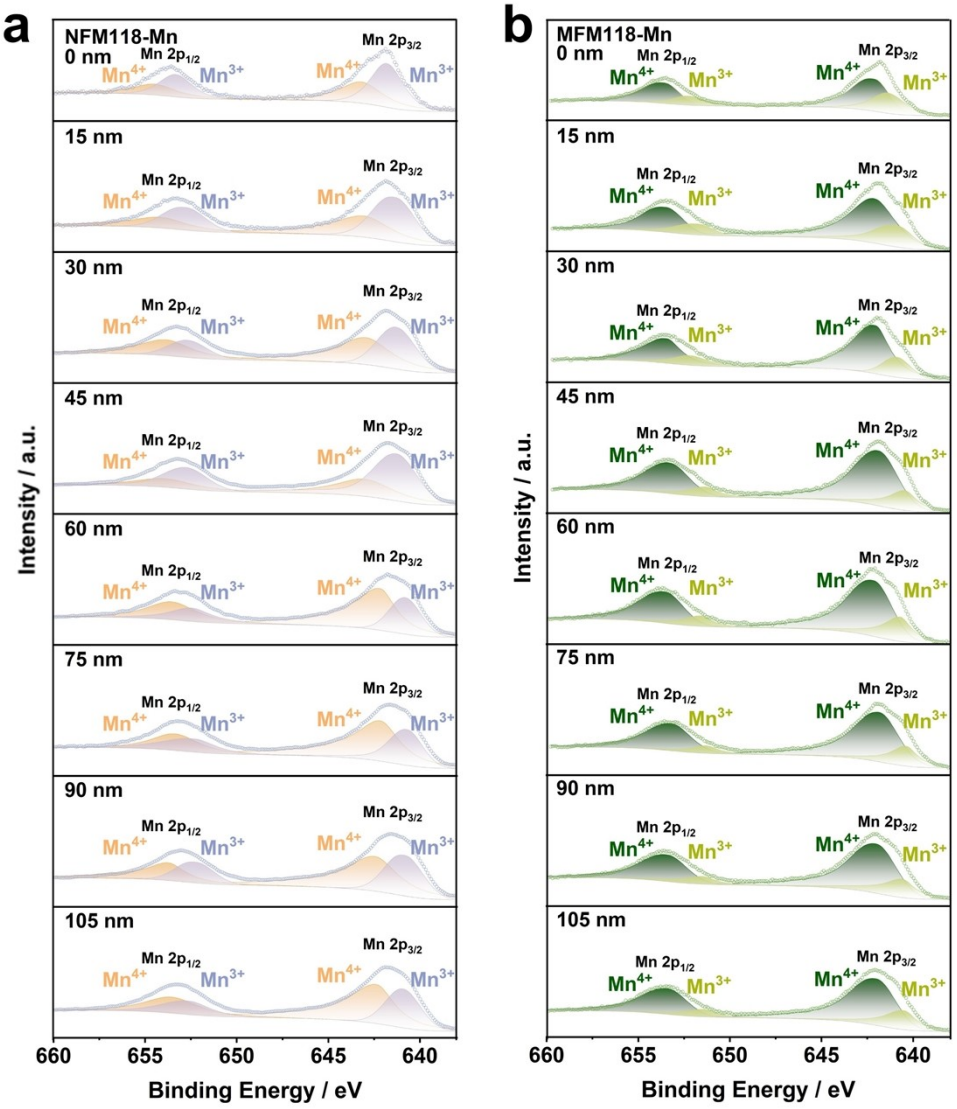

Figure S2. High resolution XPS spectra of (a) Mn 2p at surface of NFM118 pellets and (b) surface of MFM118.

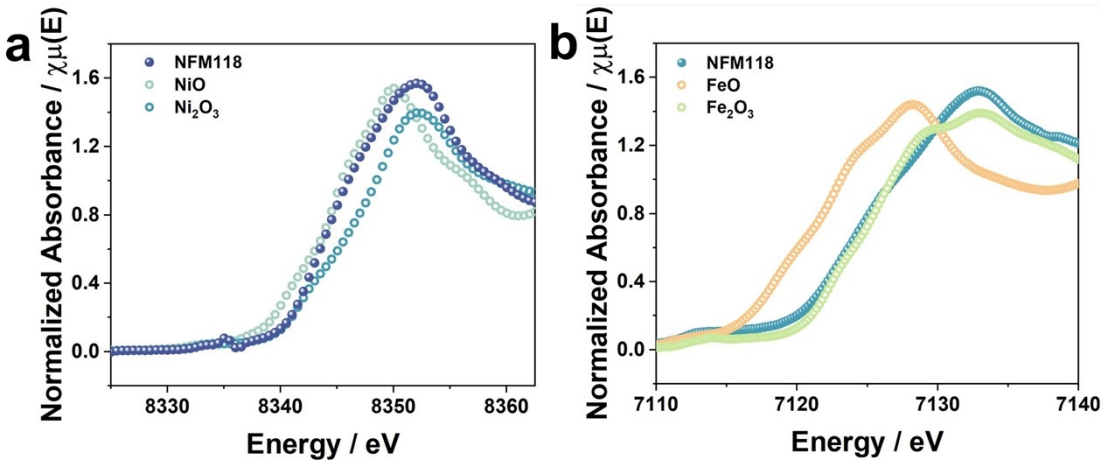

Figure S3. (a) and (b) Normalized Ni K-edge XANES spectra and normalized Fe K-edge XANES spectra of NFM118.

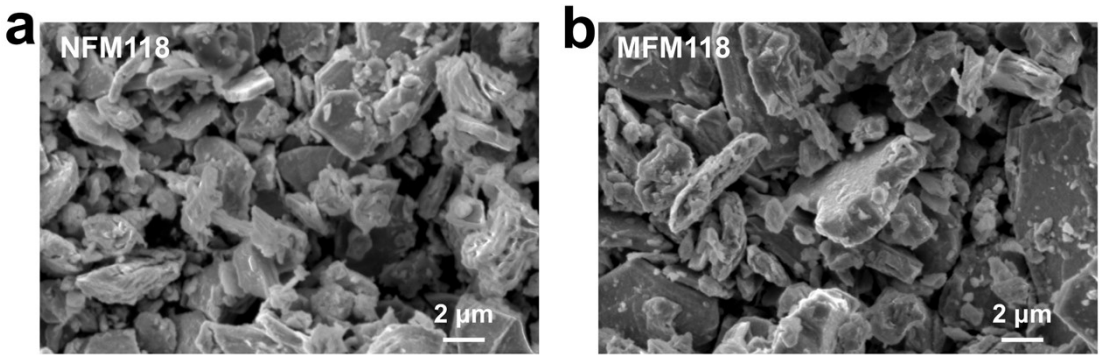

Figure S4. SEM images of (a) NFM118 and (b) MFM118.

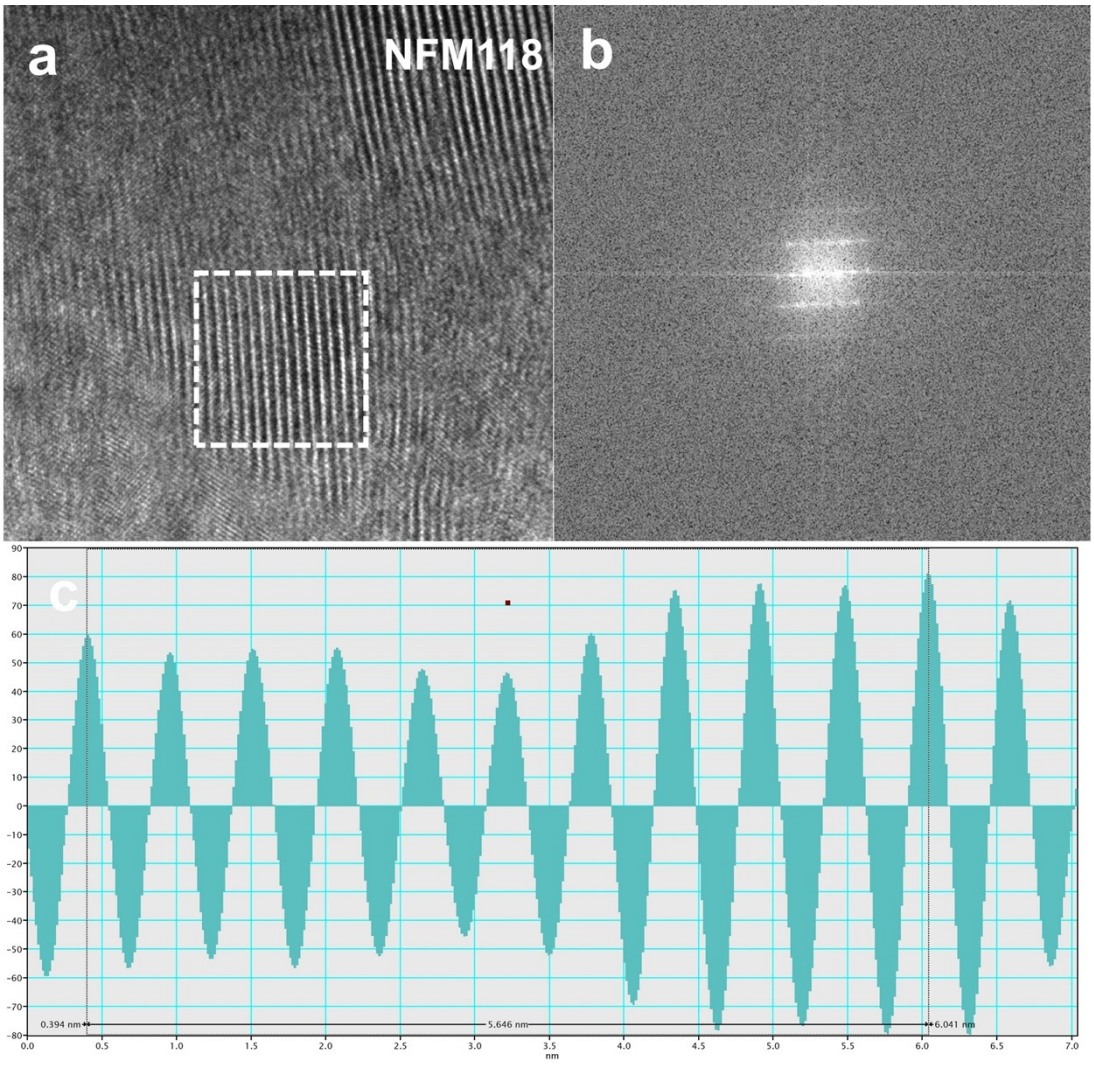

Figure S5. TEM images of (a) NFM118. (b) FFT image of TEM. (c) Line profile of the P2 structure in NFM118.

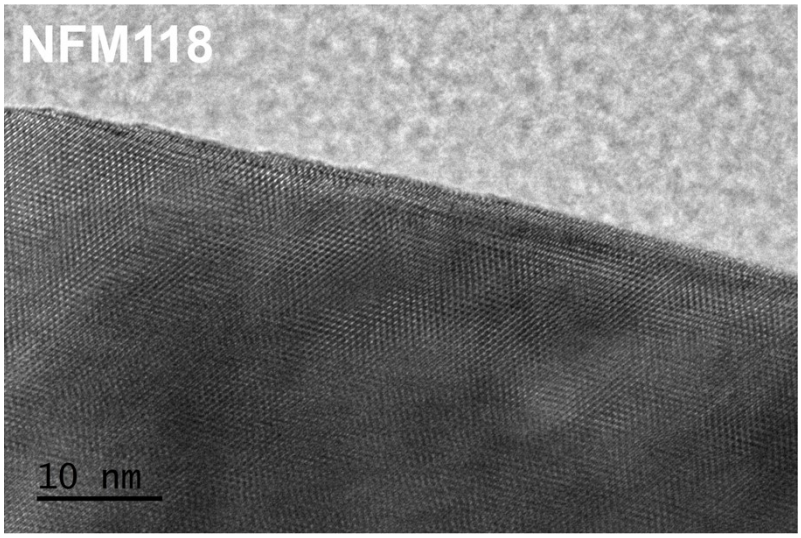

Figure S6. HRTEM image of NFM118.

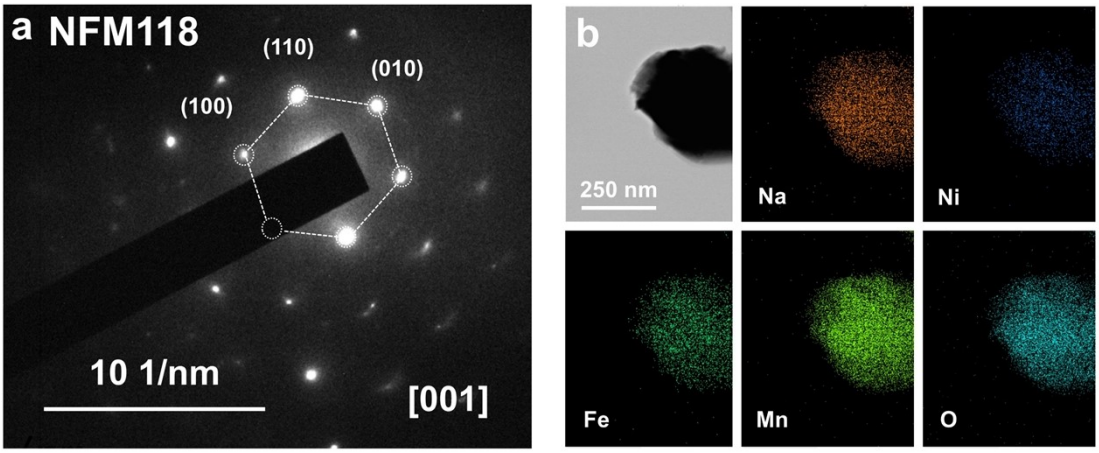

Figure S7. Structure characterization of pristine NFM118 materials. (a) SAED patterns projected from the zone axis of [001] directions. (b) STEM image of NFM118. Elements distribution of Na, Ni, Fe, Mn, and O.

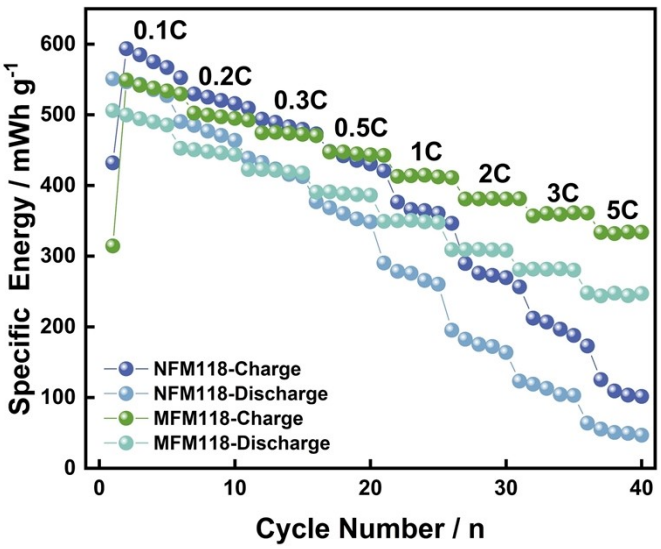

Figure S8. Rate performance of NFM118 and MFM118 in the voltage window of 1.5-4.3 V.

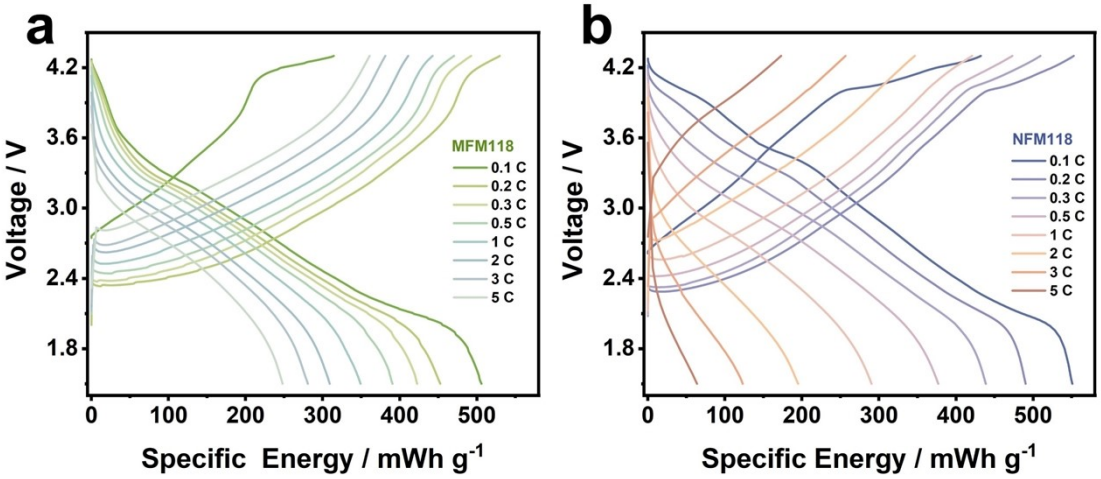

Figure S9. Charge/discharge curves of (a) NFM118 and (b) MFM118 at different rates in 1.5– 4.3 V.

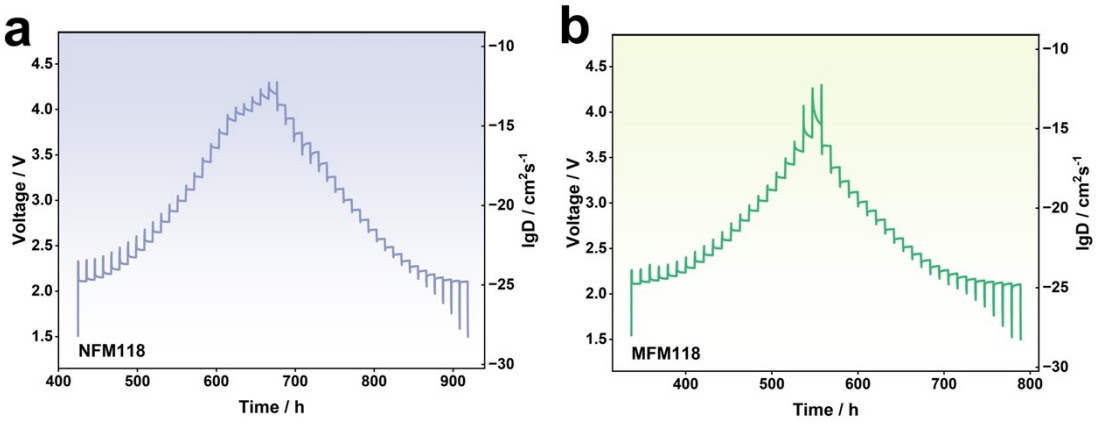

Figure S10. GITT curves of (a) NFM118 and (b) MFM118.

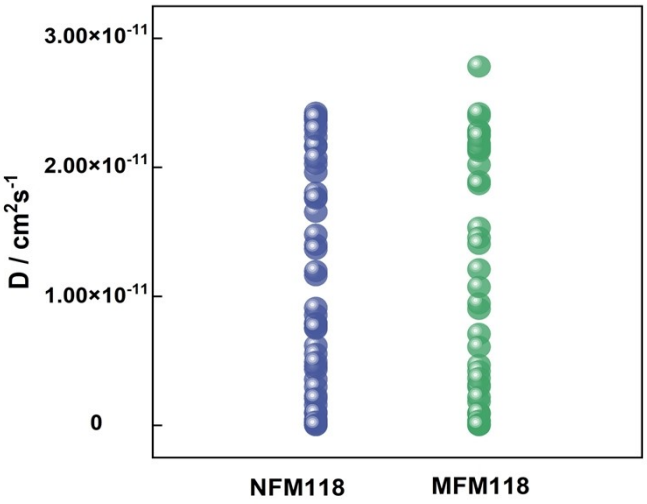

Figure S11. GITT curves of NFM118 and (b) MFM118.

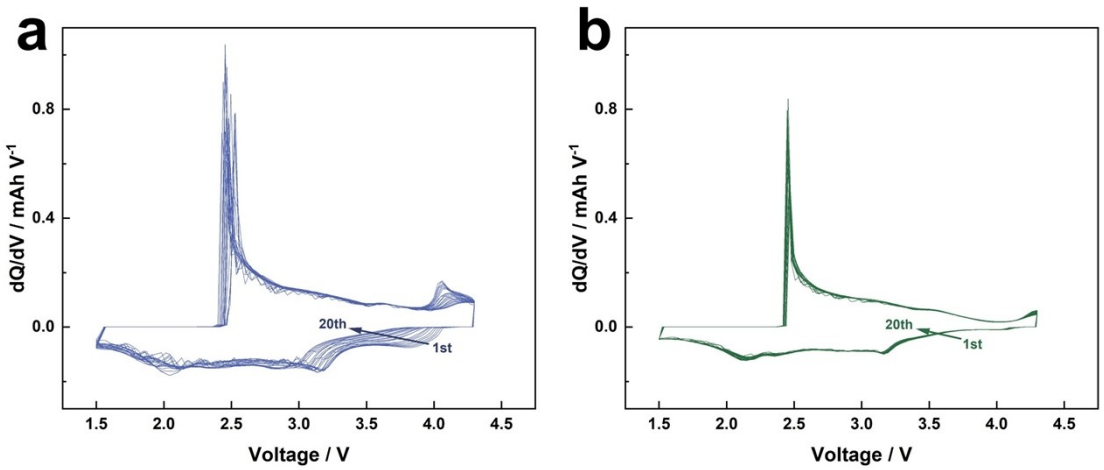

Figure S12. dQ/dV curves of (a) NFM118 and (b) MFM118 at different cycles test at 1.5-4.3 V.

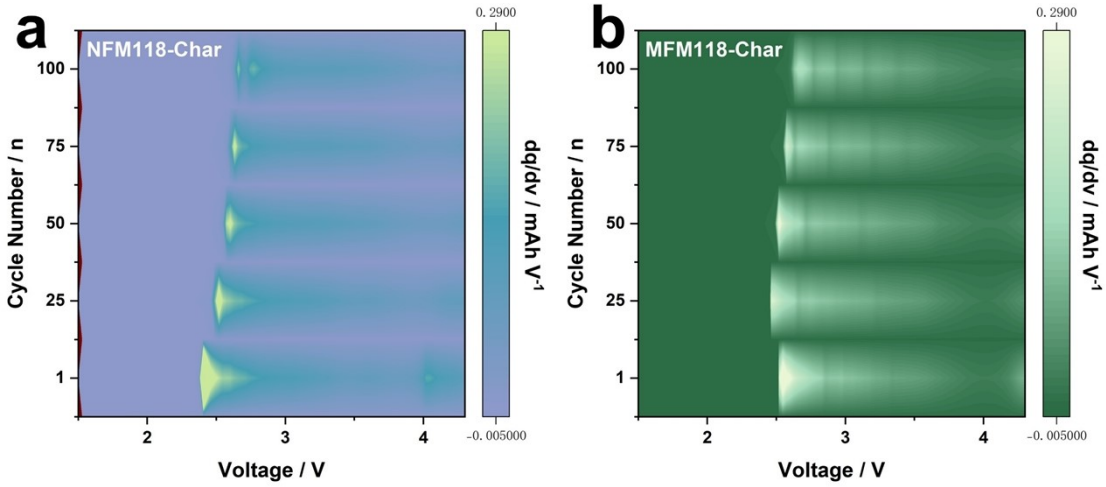

Figure S13. The dQ/dV contour plots of voltage capacity charging with different from 1.5 to 4.3 V for (a) NFM118 and (b) MFM118.

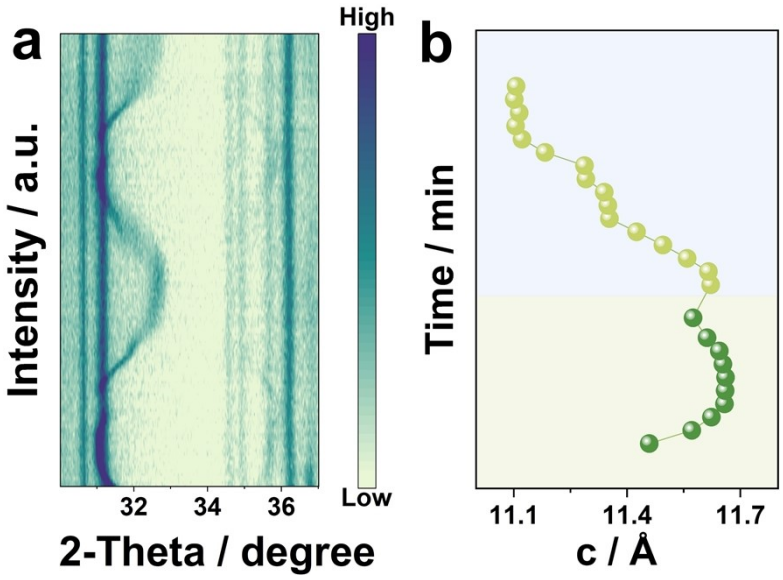

Figure S14. The 3D counter graphs of the characteristic diffraction peaks of (a) MFM118 and (b) Lattice parameters evolution.

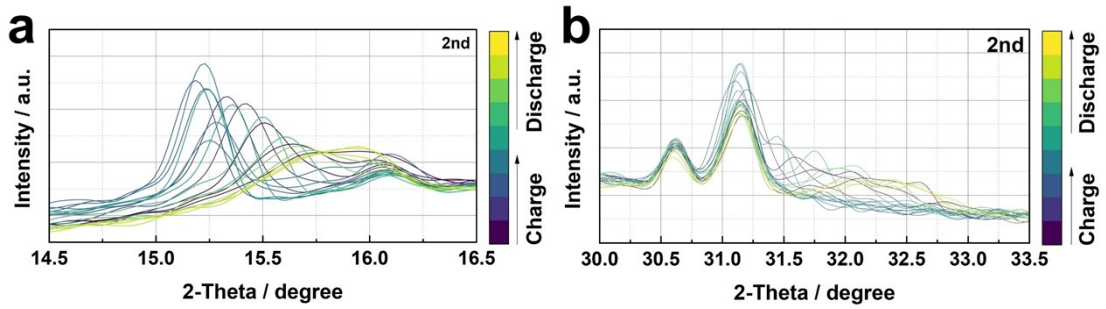

Figure S15. In situ XRD Charge/discharge curves of the evolution of characteristic diffraction peaks of (a) NFM118 and (b) MFM118.

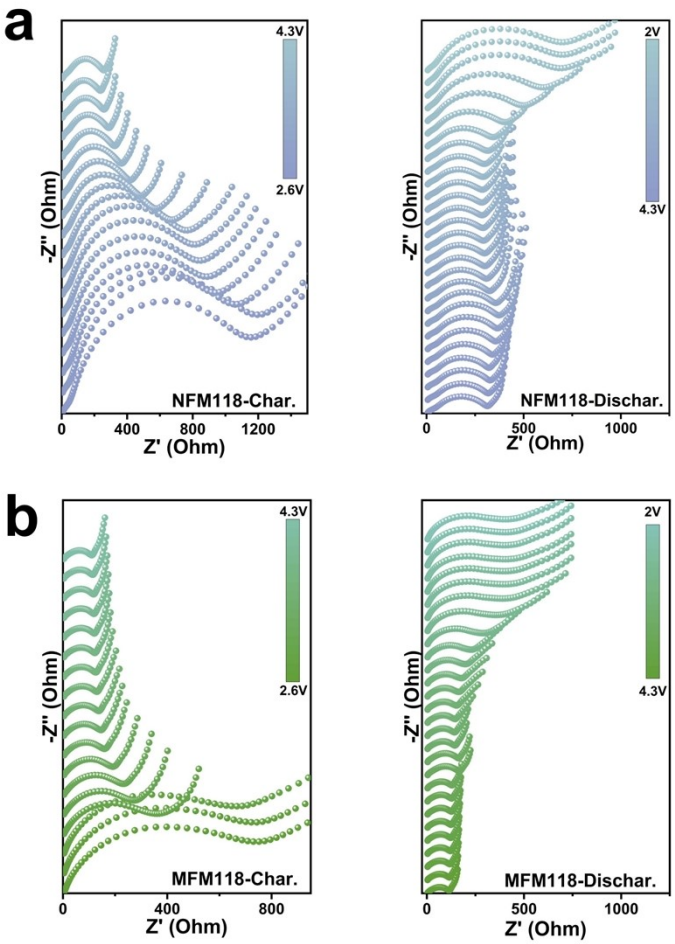

Figure S16. Detailed Semi-in situ EIS at different charge and discharge voltages. (a) NFM118 and (b) MFM118.

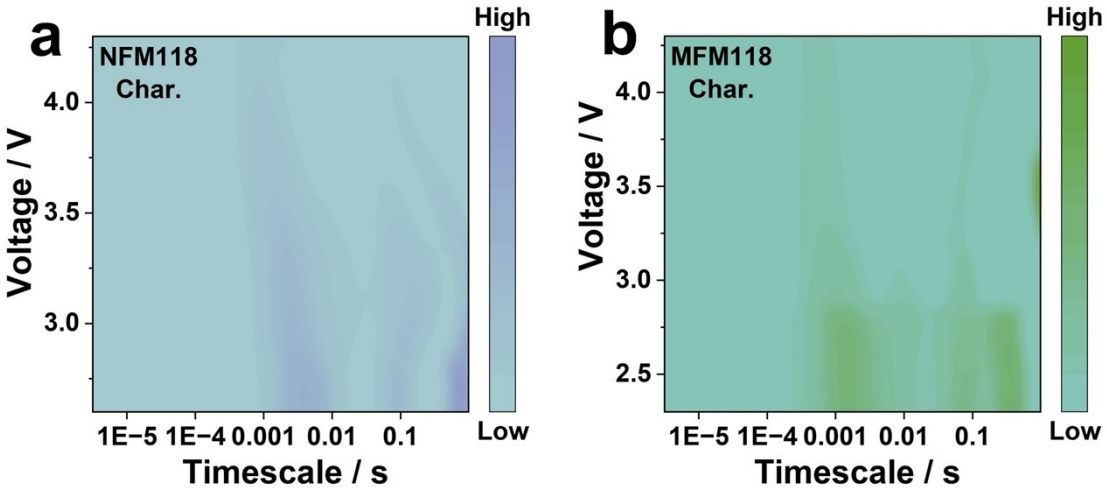

Figure S17. The 3D counter graphs of charge with the DRT for (a) NFM118 and (b) MFM118.

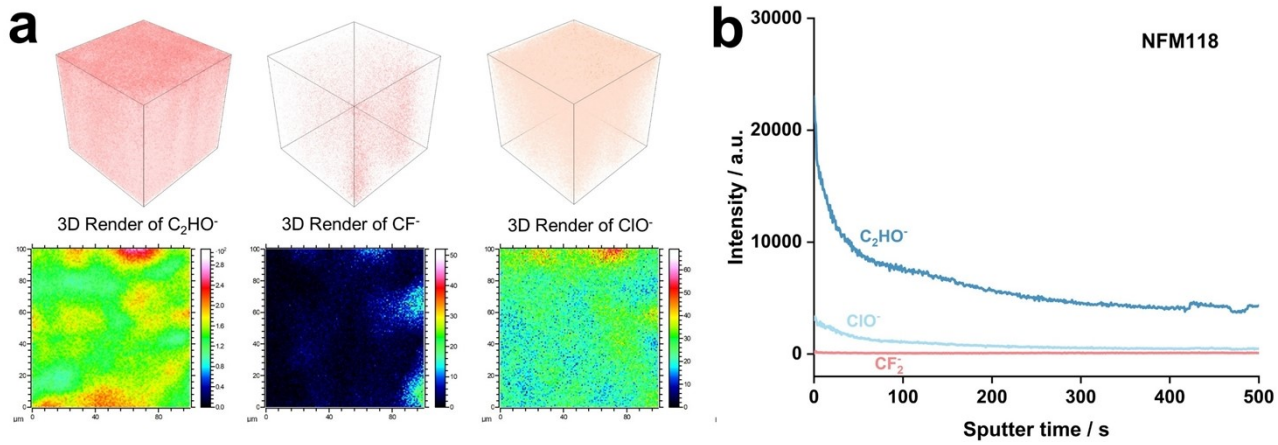

Figure S18. The 3D and 2D distributions of (a) NFM118 and (b) the TOF-SIMS depth profile of different groups.

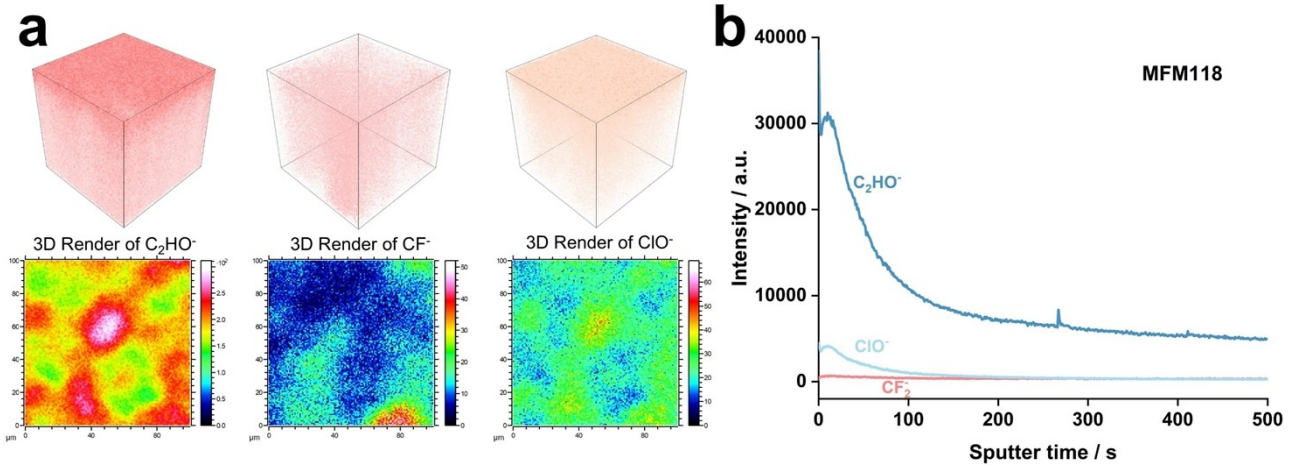

Figure S19. The 3D and 2D distributions of (a) MFM118 and (b) the TOF-SIMS depth profile of different groups.

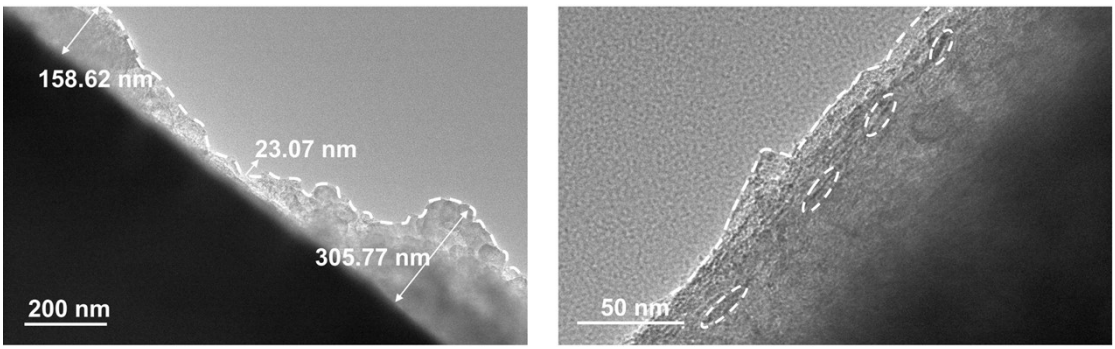

Figure S20. The TEM images of after 200 cycles for NFM118.

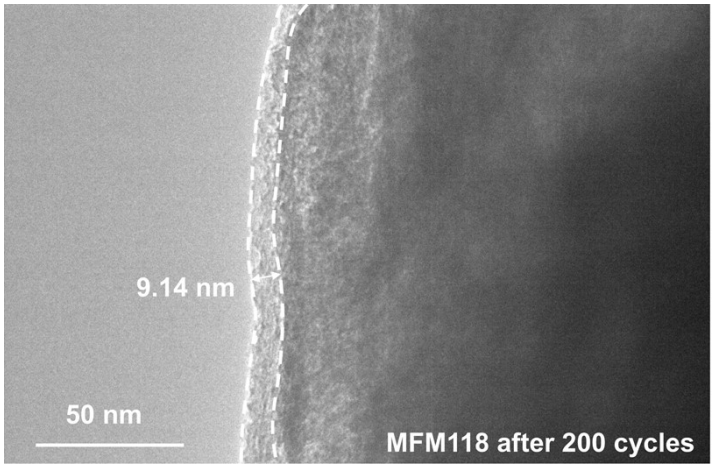

Figure S21. The TEM images of after 200 cycles for MFM118.

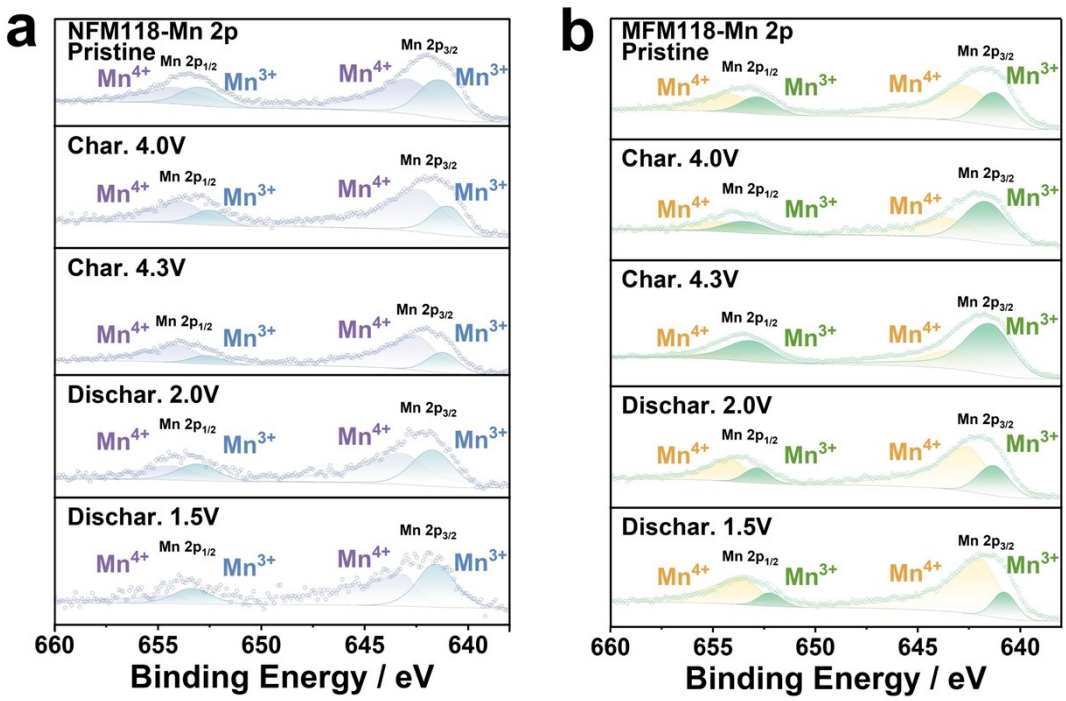

Figure S22. High resolution XPS spectra of (a) Mn 2p at different voltage of NFM118 and (b) MFM118.

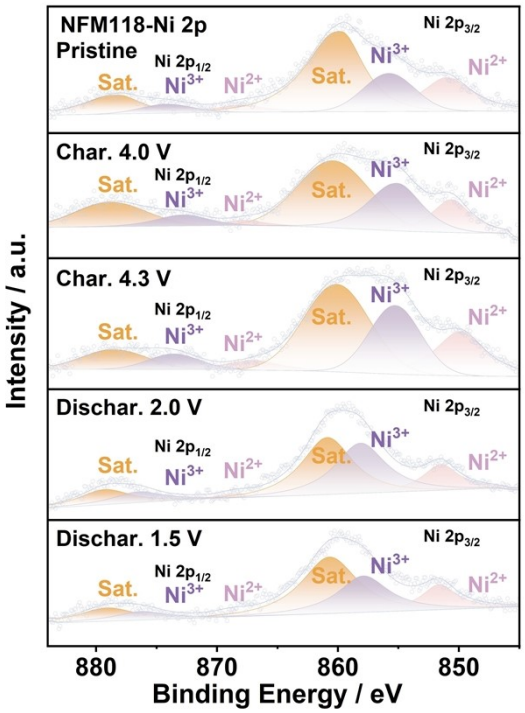

Figure S23. High resolution XPS spectra of Ni 2p at different voltage of NFM118.

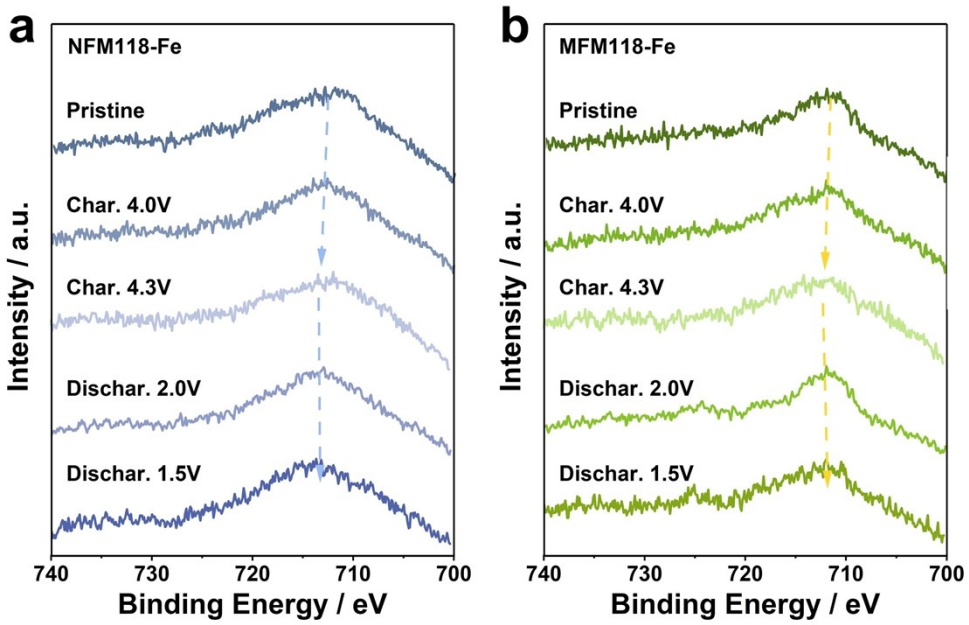

Figure S24. High resolution XPS spectra of (a) Fe 2p at different voltage of NFM118 and (b) MFM118.

Table 1. The results of linear fitting of peak current versus square root of the scan rate of NFM118 and MFM118.

Equation	**Y = a + b◊x**	
Materials	**NFM118**	**MFM118**
Number of Points	6	6
Degrees of Freedom	4	4
Residual Sum of Squares	7.02E-10	1.67E-09
Pearson's r	0.998825	0.9963
R-Square (COD)	0.99564	0.99262
Intercept Value	-1.41E-04	-1.45E-04
Intercept Standard Error	1.61E-05	2.49E-05
Slope Value	0.02441	0.02581
Slope Standard Error	7.22 E-04	1.11E-03

Table 2. Na^+ diffusion coefficients of NFM118 and MFM118.

Equation	$I_p = 0.4463n^{3/2}F^{3/2}CSR^{-1/2}T^{-1/2}D_{Na+}{}^{1/2}V^{1/2}$
Materials	Diffusion coefficient (D_{Na+})
NFM118	7.84E-12
MFM118	8.77E-12

Reference

[1] C. Cai, X. Li, J. Li, R. Yu, P. Hu, T. Zhu, T. Li, S. Lee, N. Xu, H. Fan, J. Wu, L. Zhou, L. Mai, K. Amine, *Nat. Commun.* **2025**, 16, 100.

[2] A. Joshi, A. Bano, S. Maiti, A. Krishnan, A. Kondrakov, S. Patel, R. R. Kapaev, T. K. Zakharchenko, N. Leifer, D. T. Major, D. Aurbach, M. Noked, *Adv. Energy Mater.* **2025**, n/a, e03573.

[3] Y. Li, K. A. Mazzio, N. Yaqoob, Y. Sun, A. I. Freytag, D. Wong, C. Schulz, V. Baran, A. S. J. Mendez, G. Schuck, M. Zając, P. Kaghazchi, P. Adelhelm, *Adv. Mater.* **2024**, 36, 2309842.

[4] X. Wang, Z. Yang, D. Chen, B. Lu, Q. Zhang, Y. Hou, Z. Wu, Z. Ye, T. Li, J. Lu, *Adv. Funct. Mater.* **2024**, 35, 2418322.

[5] L. Feng, Y. Xia, F. Cheng, X. Zhou, X. Xu, H. Wang, Y. Sun, W. Zhang, Y. Fan, C. Sun, W. Zha, C. Li, Y. Li, J. Peng, Y. Jiang, *Angew. Chem. Int. Ed.* **2025**, 64, e16746.